Numerical Modeling of Earth Retaining Walls Constructed in Limited Spaces

Elsamny M. Kassem[1] and Abd EL Samee W. Nashaat[2]

[1]Civil Engineering Dep., Al-Azhar University, Cairo, Egypt.
[2]Civil Engineering Dep., Faculty of Engineering, Beni- Suef University, Beni- Suef, Egypt.
waelnashat@eng.bsu.edu.eg

Abstract: The study of soil pressure against retaining wall in the case of constrained "narrow" backfill is considered highly important and of a great interested in the Geotechnical engineering. In the present study, the study of retaining wall in the case of constrained "narrow" backfill is investigated. Theoretical analysis was conducted to determine the effect of constrained "narrow" backfill on soil pressure at different backfill widths. The analysis was carried out using the Plaxis software program. Two types of retaining walls have been used in the investigation (RC and Masonry walls). In addition, the angle of constrained rock slope ranged between (β=60^o, 70^o, 80^o and 90^o) at different angles of internal friction. The obtained results were compared with the Rankine theory and arching theory. It was concluded that, the lateral earth pressure increases with increasing the constrained (narrow) backfill width and decreases with increasing the angle of rock slope. However, the coefficient of lateral earth pressure increases with increasing the constrained (narrow) backfill width and increasing with increasing width to height ratio of the wall. In addition, the lateral earth pressure coefficient (K) increases with decreasing soil friction angle (Ø) and decreases with increasing angle of rock slope (β). The lateral earth pressure coefficient (K) for masonry wall is higher than for RC wall. However, the value of the coefficient of active earth pressures (K) is found to be 0.65 to 0.85 of Rankine coefficients (K_r). In addition, the failure surface consists of a log spiral portion with a pole above the wall top and its tangent inclined with different angles to the horizontal surface. Moreover, the log spiral portion originates from the wall base with different tangent angles. In addition, the tangent of the log spiral portion that inclined with different angels to the horizontal surface depends on the soil friction angle (Ø) and angle of rock slope (β). However, the obtained results show fair agreement with the available solutions.
[Elsamny M. Kassem and Abd EL Samee W. Nashaat. **Numerical Modeling of Earth Retaining Walls Constructed in Limited Spaces.** *Life Sci J* 2019;16(1):10-24]. ISSN: 1097-8135 (Print) / ISSN: 2372-613X (Online). http://www.lifesciencesite.com. 2. doi:10.7537/marslsj160118.02.

Keywords: Retaining wall, Backfill, narrow, constrained, slope angle, rock, failure mechanism

1. Introduction

The types of retaining walls that are referred as "constrained (narrow)" backfill retaining walls are done under constrained spaces. However, the behavior of constrained retaining walls differs from that of traditional walls. In addition, the lateral earth pressure is no longer calculating by using conventional equations.

Aubertin. M. et al. (2003) estimated the response of backfill and indicated that the arching has a significant effect of the distribution of load along the wall [1].

Leshchinsky and Hu. (2003) used different wall aspect ratios at the bottom of the wall and different inclinations of the back slope. The purpose of the limit equilibrium analyses was to calculate the force required for equilibrium with the shear strength of the soil fully developed. Leshchinsky and Hu assumed circular slip surfaces [2].

Lawson and Yee (2005) showed that the horizontal earth pressures were less than or equal to the Rankine active earth pressures when the wall aspect ratio was less than or equal to 70 percent of the wall height. Lawson and Yee also showed that the horizontal earth pressure coefficient decreases as the wall aspect ratio decreases [3].

Matthias Sperl (2006) introduced a translation of Janssen's article (1895). Janssen found that the earth pressure is reduced if using arching theory. However, the arching theory could be used for granular soil with acceptable results [4].

Kniss, Ken T et al. (2007) presented an analysis on the earth pressure distribution against the wall in constrained "narrow" spaces. Kniss, Ken T et al found that the arching theory effect is conservative [5].

Kuo-Hsin Yang and Chia-Nan Liu (2007) conducted an analysis on the distribution of earth pressure against constrained "narrow" backfill retaining wall. Kuo-Hsin Yang and Chia-Nan Liu found that the earth pressure increases with increasing wall aspect ratio and that in case the arching effect is taken into consideration. In addition, Kuo-Hsin Yang and Chia-Nan Liu found that the conventional earth pressure theories are over estimated to be used in narrow backfill retaining wall [6].

Kame. et al. (2010) presented a method based on the application of Kötter's equation proposed for the complete analysis of active earth pressure on a vertical

wall retaining sand backfill. The log spiral failure surface was assumed [7].

Eltayeb H. O. (2015) presented experimentally the evaluation of the reaction induced by lateral earth pressure from granular soil contained between two parallel rigid retaining walls [8].

Gihan Abdelrahman. et al. (2017) presented a study using a finite element theoretical analysis. A limit equilibrium analysis was presented using Geo-Studio 2007 program (Slope/W Design) to discuss the behavior of narrow MSE wall as a function of aspect ratio, reinforcing elements spacing. In addition, the study presents the effect of varying aspect ratio, L/H, of narrow MSE wall on location and shape of failure surface. It was found that by increasing the aspect ratio of the wall would result in increasing the factor of safety [9].

The purpose of the present study is to investigate the effect of the constrained backfill properties and dimensions on the distribution of lateral earth pressure on retaining wall as well as the coefficient of lateral earth pressure. In addition, determine the failure mechanism due to constrained (narrow) backfill. The selected backfill is horizontal cohesionless soil.

2. Theoretical Analysis

Finite element method using the PLAXIS 2D was selected to develop numerical models to study the failure mechanism due to constrained backfill. In addition, determine the relationship between the backfill properties, dimensions and the lateral earth pressure coefficient.

3. Numerical Program

The main purpose of this study was to investigate the failure mechanism of constrained backfill retaining wall and the relationship between the coefficient of lateral earth pressure and backfill properties, dimensions. Two types of retaining wall have been used in the investigation (RC and Masonry walls). The typical geometry of the backfill used in the present study is shown in Figs (1) and (2). The walls used in the analyses a rigid. The analysis program and the used properties for the backfill, the rock, and walls used in the analyses are listed in Table (1) and Table (2). Figs (1) and (2) show the retaining wall's dimensions with backfill space (b) ranged from 40, 50, 60 to 70 cm and the angle of rock slope (β) ranged from 60^o, 70^o,80^o to 90^o. The angle of internal friction of back fill sandy soil used is ranged from 30^0, 32^0, 34^0, 36^0 to 38^0. A semi-infinite element isotropic homogeneous elastic material simulates the soil and the material model used is Mohr-Coulomb, while the concrete and masonry simulated as rigid material.

Table (1) Investigated cases of study by numerical analysis program.

Retaining Wall	Retaining wall height (H) m	Angle of Internal Friction (Ø)	Backfill Dimensions: Distance of back fill at top of wall (S) S=b+H*tan (90–β)^o S=b+(D-d)+H*tan (90-β)^o				Backfill Dimensions: Distance of back fill at bottom of wall (b) m	Angle of rock slope (β)
Rc. Wall	4.5	30^0, 32^0, 34^0, 36^0 and 38^0	0.4	1.2	2.0	3.0	0.40	60^o
			0.5	1.3	2.1	3.1	0.50	70^o
			0.6	1.4	2.2	3.2	0.60	80^o
			0.7	1.5	2.3	3.3	0.70	90^o
Masonry wall	4.5	30^0, 32^0, 34^0, 36^0 and 38^0	1.1	1.9	2.7	3.7	0.40	60^o
			1.2	2.0	2.8	3.8	0.50	70^o
			1.3	2.1	2.9	3.9	0.60	80^o
			1.4	2.2	3.0	4.0	0.70	90^o

Where: H: Retaining wall height. D: bottom width of retaining wall. d: top width of retaining wall.
β: Angle of rock slope. b: limited backfill space. S: Space of back fill at top of wall.

Table (2) The used properties for the backfill, the rock, and walls.

Parameters	Backfill Soil	Rock	Retaining wall
Material Model	Mohr - Coulomb	Linearly elastic	Linearly elastic
Type of Material	Sand	Rock	Concrete\ Masonry
Unit weight, γ (kN/m^3)	17.5	22	25\18
Young's modulus, E_s (kN/m^2)	20000	200000	210000\180000
Poisson's ratio, υ	0.3	0.1	0.1\0.15
cohesion, C_u (kN/m^2)	0	400	--
Friction angle, Ø (deg)	30^0, 32^0, 34^0 and 36^0	45	--
Dilatancy angle, ¥ (deg) [Ø-30]	0, 2, 4 and 6	--	--

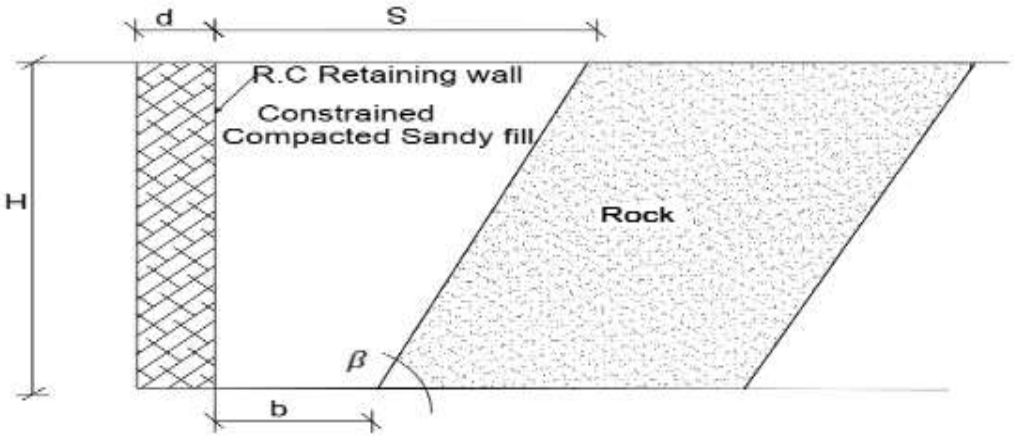

Fig (1). Geometry of backfill and Rc retaining wall.

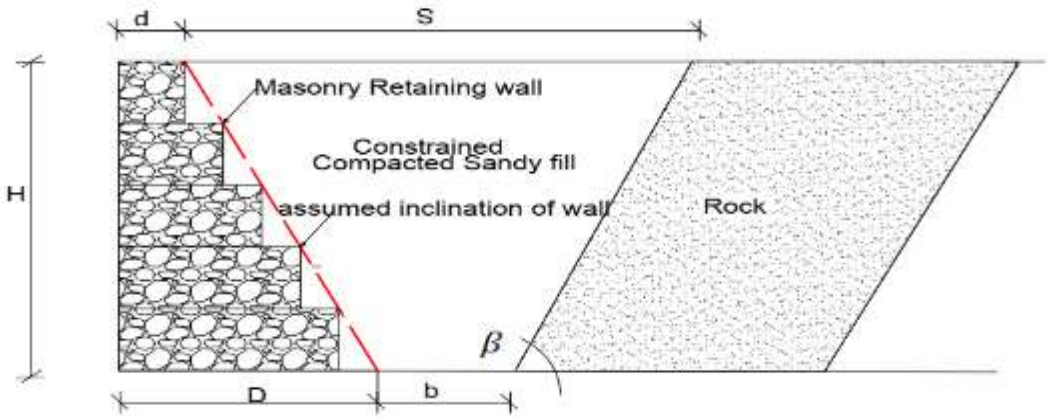

Fig (2). Geometry of backfill and Masonry retaining wall.

3-1) Finite Element Models

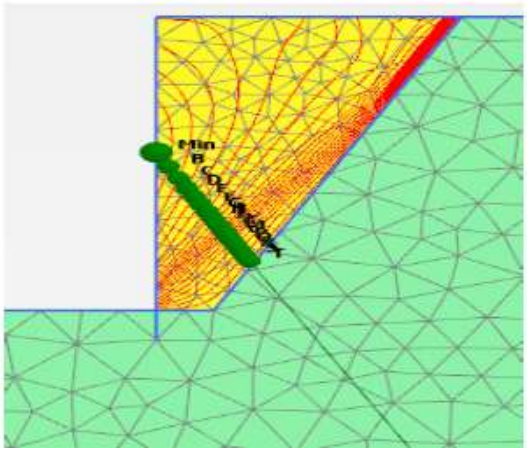

Fig (3) Stress distribution and finite element mesh for RC retaining wall with backfill space (b=0.40m and ß=60o).

A finite element model was developed to investigate the lateral earth pressure effect on retaining wall in the case of constrained backfill. Figs (3) to (10) show some examples of finite element output for retaining walls (RC wall, and Masonry wall) with limited backfill spaces.

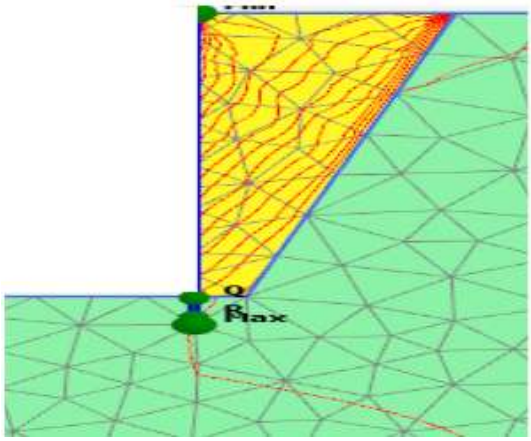

Fig (4) Stress distribution and finite element mesh for RC retaining wall with backfill space (b=0.40m and ß=70o).

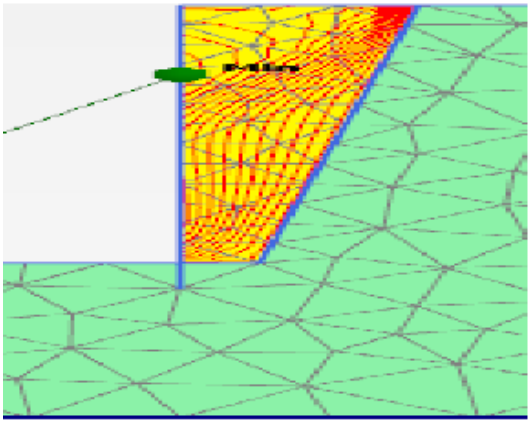

Fig (5) Stress distribution and finite element mesh for RC retaining wall with backfill space (b=0.40m and ß=80o).

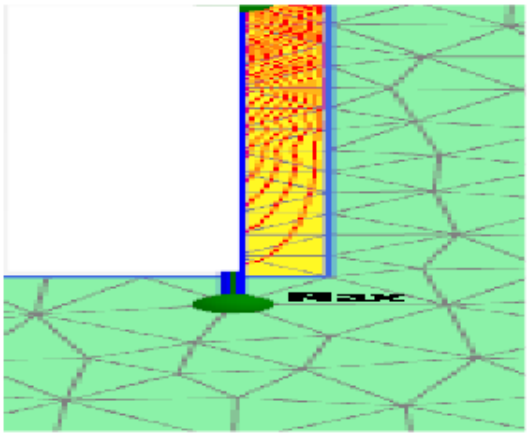

Fig (6) Stress distribution and finite element mesh for RC retaining wall with backfill space (b=0.40m and ß=90o).

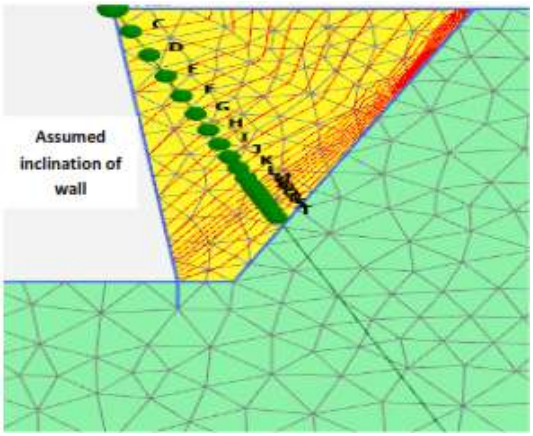

Fig (7) Stress distribution and finite element mesh mesh for masonry retaining wall with backfill space (b=0.40m and ß=60o).

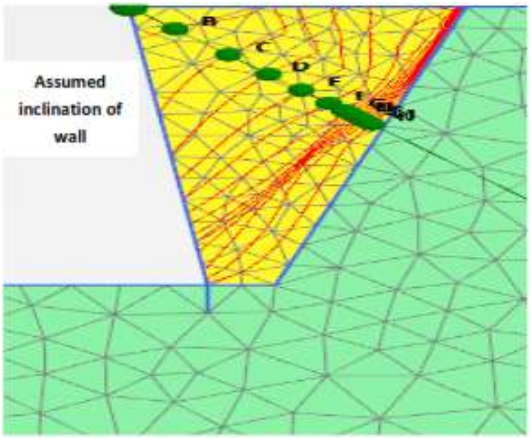

Fig (8) Stress distribution and finite element for masonry retaining wall with backfill space (b=0.40m and ß=70o).

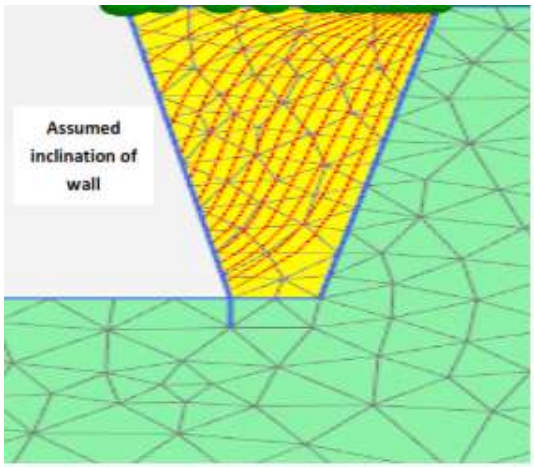

Fig (9) Stress distribution and finite element mesh for masonry retaining wall with backfill space (b=0.40m and ß=80o).

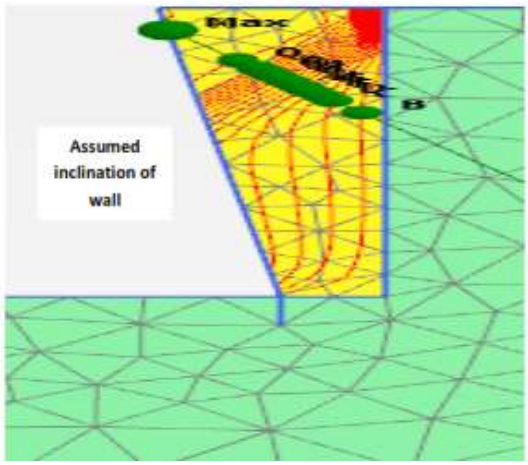

Fig (10) Stress distribution and finite element for masonry retaining wall with backfill space (b=0.40m and ß=90).

4. Analysis of Results

From the numerical analysis, two main factors were taken into consideration, the backfill dimensions and the soil friction angles. Different backfill width (b) ranging between 0.4 to 0.7 m were modeled to calculate the soil pressure against a retaining wall. For each backfill width, the soil friction angle has different magnitude values ranging between 30^0-38^0. However, the followings output are obtained:-

4.1) Distribution of Earth Pressures Along Retaining Wall Height

Based on the results obtained from numerical modeling it is clearly shown that the normalized earth pressure on retaining walls increases with depth as shown in Fig (11).

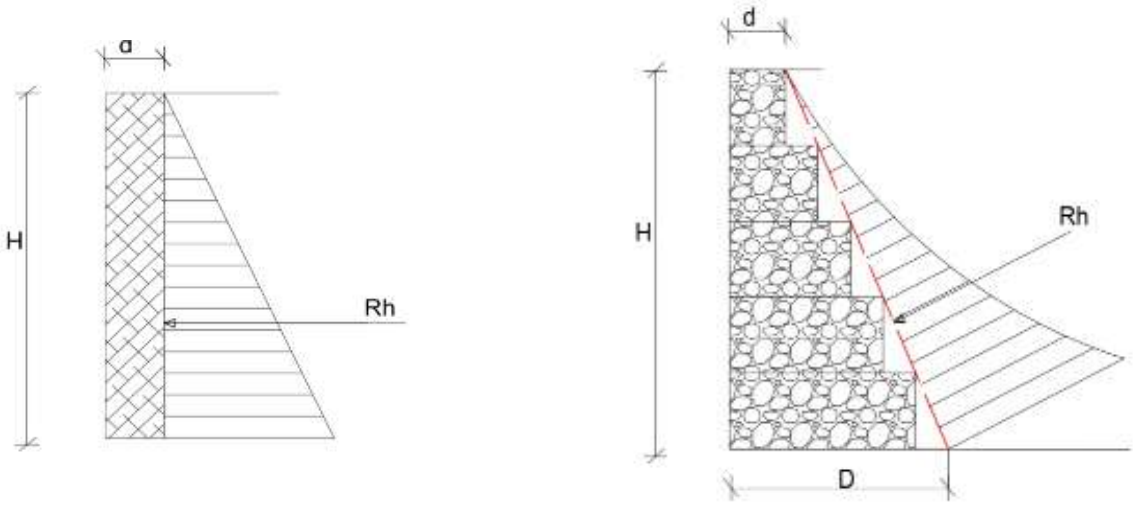

a) Earth pressure distribution on R.C wall **b) Earth pressure distribution on masonry wall**

Fig. (11) Earth pressure distribution on wall based on numerical modeling.

4.2) Effect of Backfill Dimensions on Lateral Earth Pressure

The lateral earth pressure has been determined from finite element analysis. Figs (12) to (17) show some examples of the relation between the lateral earth pressure and backfill width for RC and masonry walls at different soil friction angles and different angles of rock slope. Figs (18) to (21) show some examples of the relation between the lateral earth pressure and angles of rock slope for RC and masonry walls at different soil friction angles and different backfill widths.

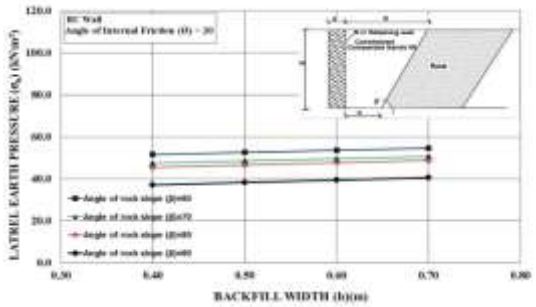

Fig. (12) The relation between the lateral earth pressure and backfill width at soil friction angle (Ø) $=30^0$ at different angles of rock slope for RC wall.

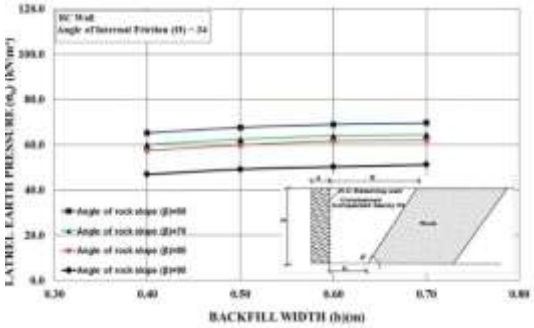

Fig. (13) The relation between the lateral earth pressure and backfill width at soil friction angle (Ø) $=34^0$ at different angles of rock slope for RC wall.

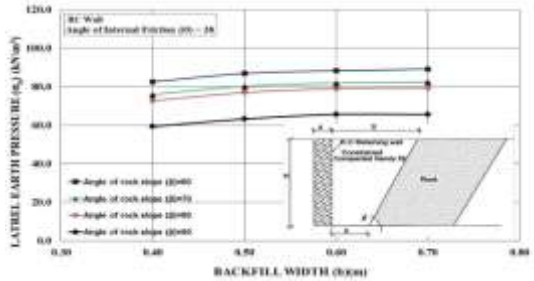

Fig. (14) The relation between the lateral earth pressure and backfill width at soil friction angle (Ø) $=38^0$ at different angles of rock slope for RC wall.

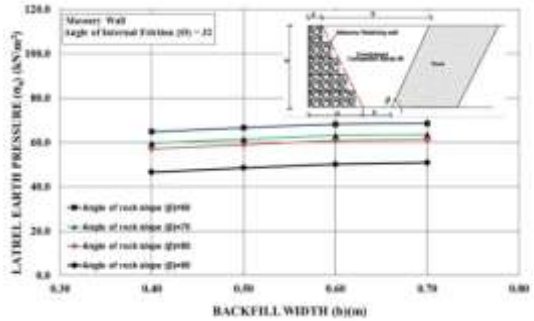

Fig. (15) The relation between the lateral earth pressure and backfill width at soil friction angle (Ø) $=32^0$ at different angles of rock slope for masonry wall.

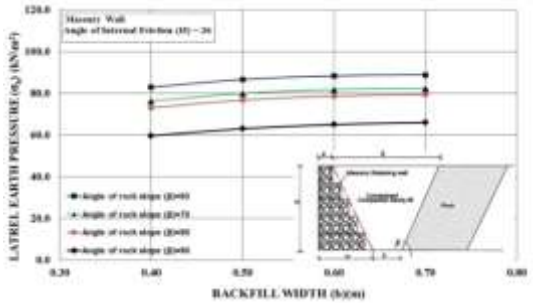

Fig. (16) The relation between the lateral earth pressure and backfill width at soil friction angle (Ø) $=36^0$ at different angles of rock slope for masonry wall.

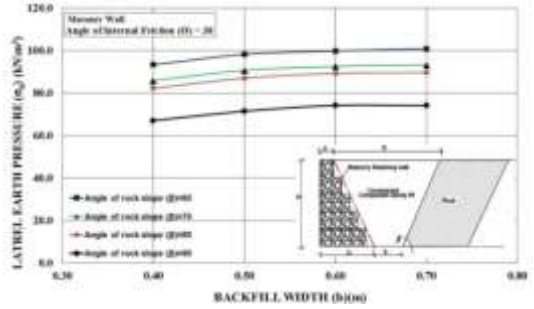

Fig. (17) The relation between the lateral earth pressure and backfill width at soil friction angle (Ø) $=36^0$ at different angles of rock slope for masonry wall.

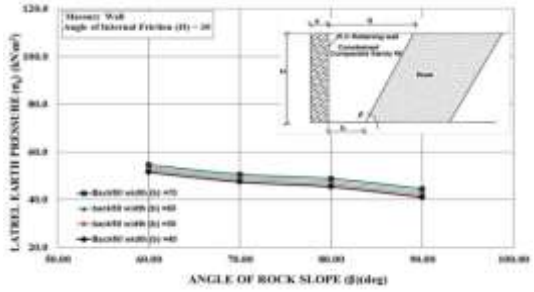

Fig. (18) The relation between the lateral earth pressure and angle of rock slope at soil friction angle (Ø) $=30^0$ and at different backfill widths for RC wall.

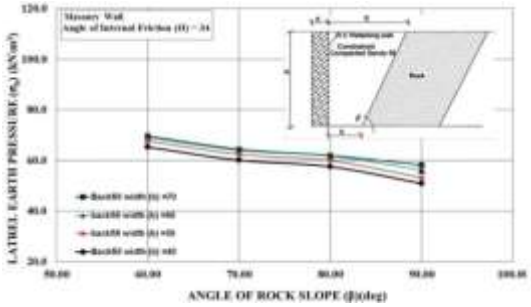

Fig. (19) The relation between the lateral earth pressure and angle of rock slope at soil friction angle (Ø) $=34^0$ and at different backfill widths for RC wall.

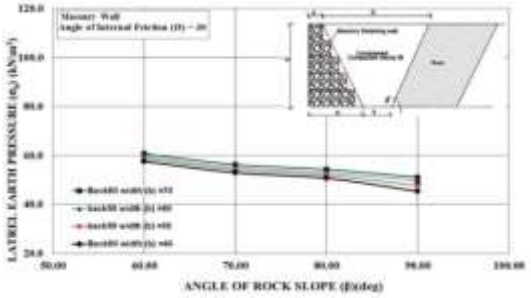

Fig. (20) The relation between the lateral earth pressure and angle of rock slope at soil friction angle (Ø) $=30^0$ and at different backfill widths for masonry wall.

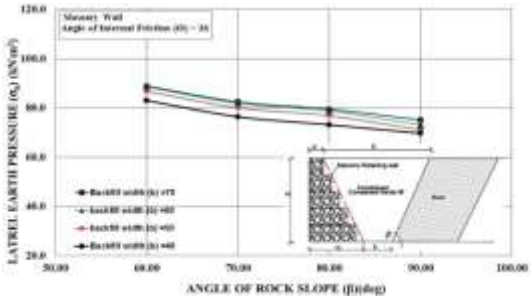

Fig. (21) The relation between the lateral earth pressure and angle of rock slope at soil friction angle (Ø) $=36^0$ and at different backfill widths for masonry wall.

From the above-obtained results, it is concluded that the lateral earth pressure increases with increasing the backfill width and decreases with increasing the slope angle of rock (β).

4.3) Backfill Dimensions Effect On Lateral Earth Pressure Coefficient

The lateral earth pressure coefficients have been obtained from finite element analysis. However, a comparison between the coefficients of lateral earth

pressures (K) obtained from the F.E analyses and Rankine theory as well as Arching theory is presented in Figs (22) to (29).

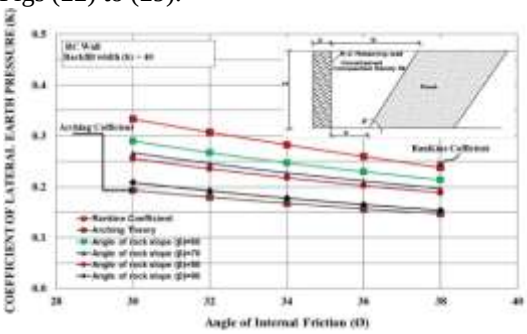

Fig. (22) The relation between soil friction angle and the coefficient of lateral earth pressure for different values of angle of rock slope β, at the backfill width (b) =40 cm for RC wall.

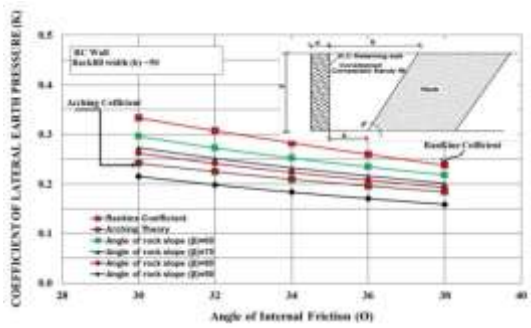

Fig. (23) The relation between soil friction angle and the coefficient of lateral earth pressure for different values of angle of rock slope β, at the backfill width (b) =50 cm for RC wall.

Fig. (24) The relation between soil friction angle and the coefficient of lateral earth pressure for different values of angle of rock slope β, at the backfill width (b) =60 cm for RC wall.

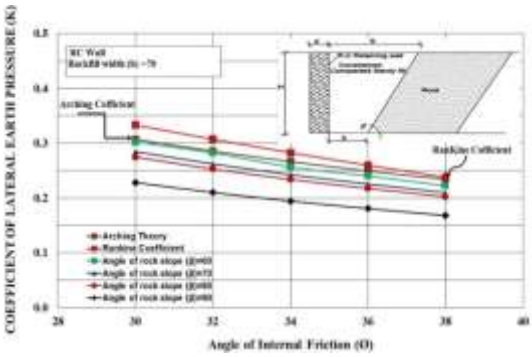

Fig. (25) The relation between soil friction angle and the coefficient of lateral earth pressure for different values of angle of rock slope β, at the backfill width (b) =70 cm for RC wall.

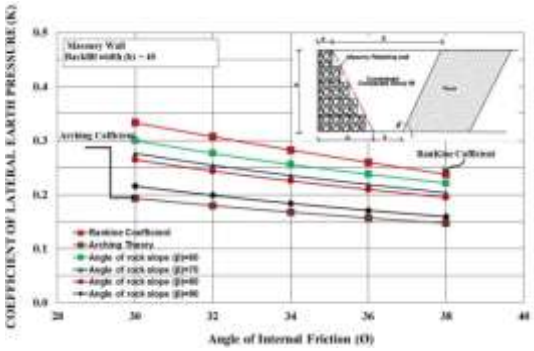

Fig. (26) The relation between soil friction angle and the coefficient of lateral earth pressure for different values of ngle of rock slope β, at the backfill width (b) =40 cm for masonry wall.

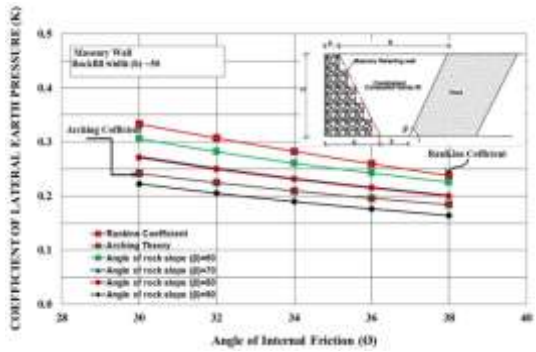

Fig. (27) The relation between soil friction angle and the coefficient of lateral earth pressure for different values of angle of rock slope β, at the backfill width (b) =50 cm for masonry wall.

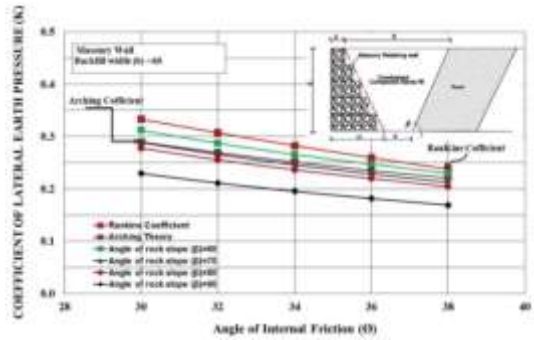

Fig. (28) The relation between soil friction angle and the coefficient of lateral earth pressure for different values of angle of rock slope β, at the backfill width (b) =60 cm for masonry wall.

Based on these results, the lateral earth pressure coefficient decreases as angle of rock slope (β) and soil friction angle (Ø) increases and increasing with increasing the backfill width (b). The magnitude value of the coefficient of lateral earth pressures (K) is found to be 0.65 to 0.85 from Rankine coefficients (Kr)

depending on rock slope angle (β). Fair agreement has been obtained with Arching theory coefficient.

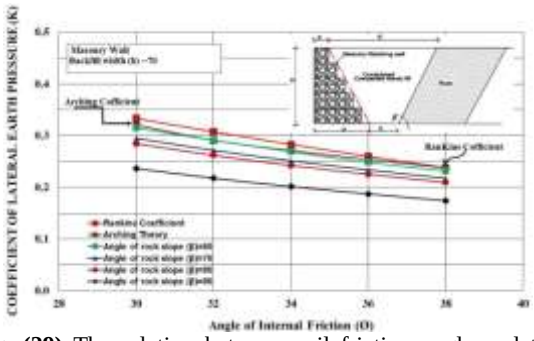

Fig. (29) The relation between soil friction angle and the coefficient of lateral earth pressure for different values of angle of rock slope β, at the backfill width (b) =70 cm for masonry wall.

4.4) Effect of Backfill Width to Height Ratio (B/H) on of Lateral Earth Pressure

The main factor governing the coefficient of lateral earth pressures (K) is the width to height ratio (b/H). The study cases of backfill width to height ratio behind retaining wall (b/H) are listed in Table (3).

Table (3) The backfill width to height ratio behind retaining wall (b/H) used in the FE analyses.

No.	Case Name	width to height ratio
1	Case 1	0.20
2	Case 2	0.40
3	Case 3	0.60
4	Case 4	0.80
5	Case 5	1.00

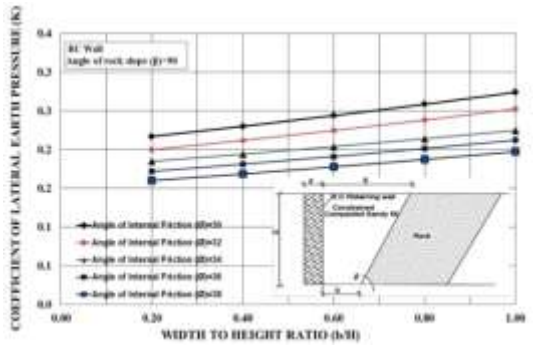

Fig. (30) The relationship between the coefficient of lateral earth pressures (K) and width to height ratio (b/H) at angle of rock slope $\beta=90^0$ for RC wall.

The relationships between the coefficient of lateral earth pressures (K) and width to height ratio (b/H) are shown in figs (30) to (37). Figs (38) and (41) show the relationship between the coefficient of active earth pressures (K) and width to height ratio (b/H) at different soil friction angle (Ø) and at different angles of rock slope for RC and Masonry wall.

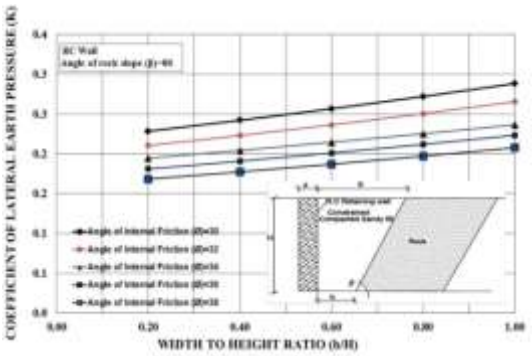

Fig. (31) The relationship between the coefficient of lateral earth pressures (K) and width to height ratio (b/H) at angle of rock slope $\beta=80^0$ for RC wall.

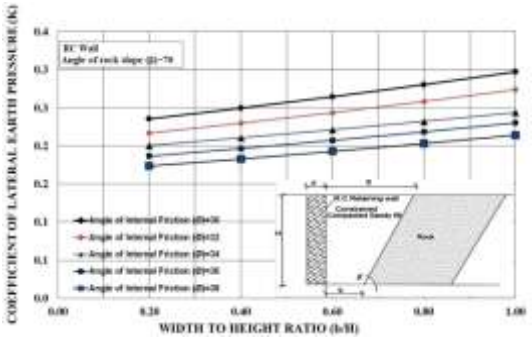

Fig. (32) The relationship between the coefficient of lateral earth pressures (K) and width to height ratio (b/H) at angle of rock slope $\beta=70^0$ for RC wall.

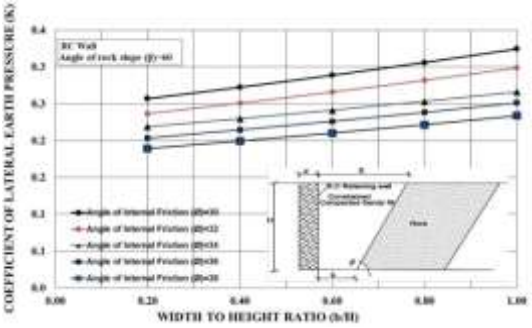

Fig. (33) The relationship between the coefficient of lateral earth pressures (K) and width to height ratio (b/H) at angle of rock slope $\beta=60^0$ for RC wall.

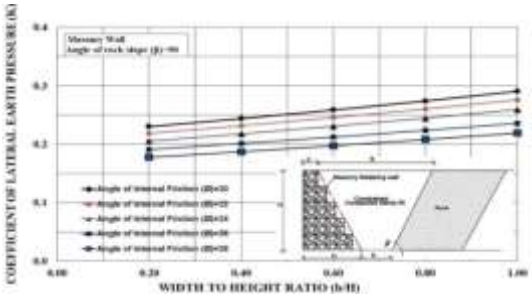

Fig. (34) The relationship between the coefficient of lateral earth pressures (K) and width to height ratio (b/H) at angle of rock slope $\beta=90^0$ for Masonry wall.

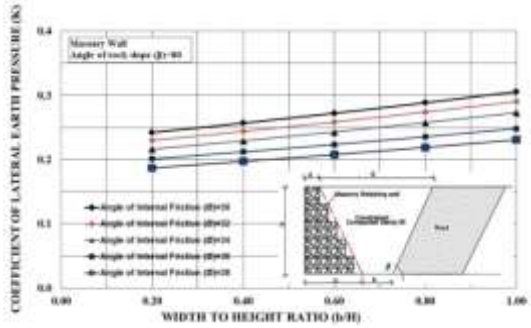

Fig. (35) The relationship between the coefficient of lateral earth pressures (K) and width to height ratio (b/H) at angle of rock slope $\beta=80^0$ for Masonry wall.

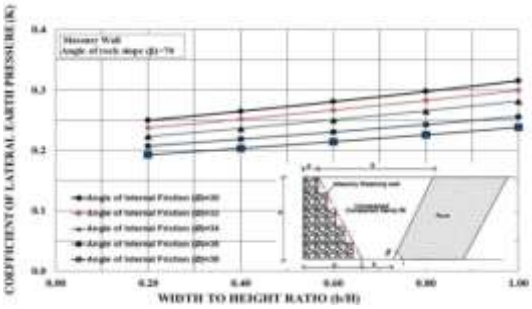

Fig. (36) The relationship between the coefficient of lateral earth pressures (K) and width to height ratio (b/H) at angle of rock slope $\beta=70^0$ for Masonry wall.

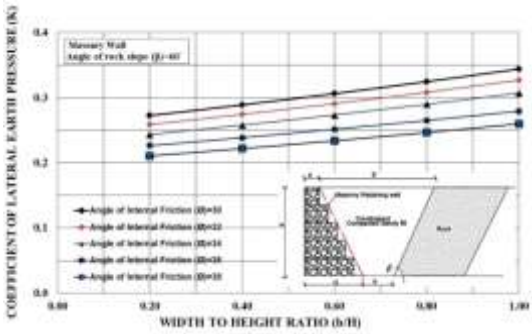

Fig. (37) The relationship between the coefficient of lateral earth pressures (K) and width to height ratio (b/H) at angle of rock slope $\beta=60^0$ for Masonry wall.

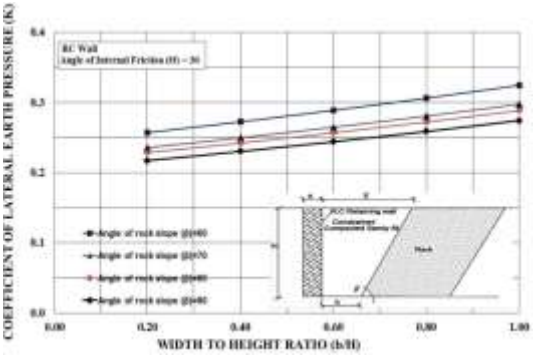

Fig. (38) The relationship between the coefficient of lateral earth pressures (K) and width to height ratio (b/H) at soil friction angle (Ø)= 30 at different angle of rock slope (β)for RC wall.

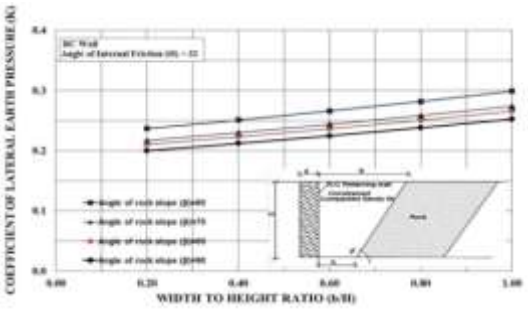

Fig. (39) The relationship between the coefficient of lateral earth pressures (K) and width to height ratio (b/H) at soil friction angle (Ø)= 32 at different angle of rock slope (β) for RC wall.

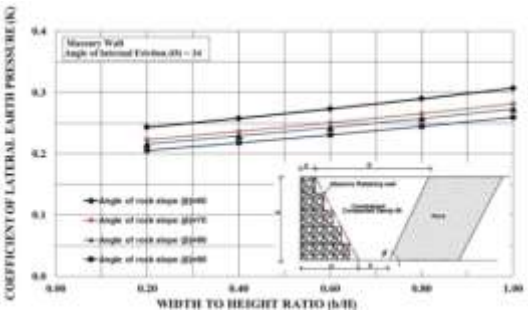

Fig. (40) The relationship between the coefficient of active earth pressures (K) and width to height ratio (b/H) at soil friction angle (Ø)=34 at different angle of rock slope for Masonry wall.

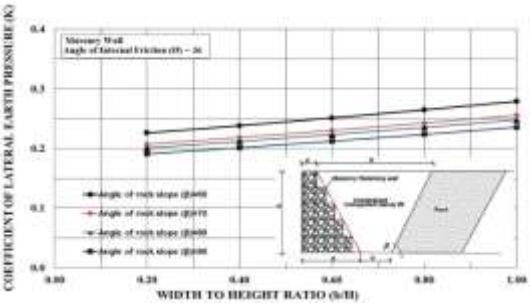

Fig. (41) The relationship between the coefficient of active earth pressures (K) and width to height ratio (b/H) at soil friction angle (Ø)=36 at different angle of rock slope for Masonry wall.

From these results, it is concluded that the lateral earth pressure coefficient (K) increases with increasing width to height ratio (b/H) and decreasing soil friction angle (Ø). In addition, lateral earth pressure coefficient (K) for masonry wall is higher than for RC wall.

5. Failure Mechanism of Constrained "Narrow" Backfill

5.1) Shape of the Failure Mechanism Obtained from Finite Element

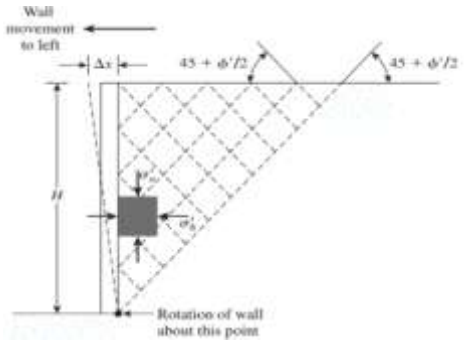

Fig. (42) Rankine's active pressure [(Das, 2011)] [10].

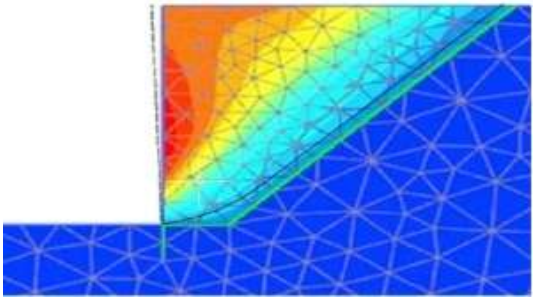

Fig. (43). Failure mechanism of retaining wall with backfill width (b=60) cm at soil friction angle Ø=300 and at angle of rock slope ß=600 for R.C wall

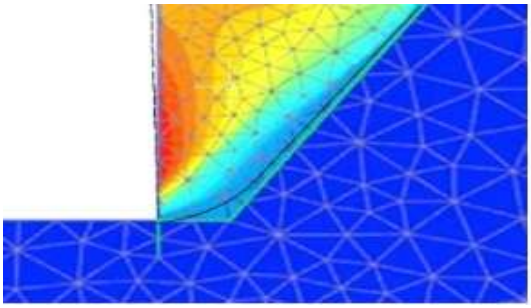

Fig. (44). Failure mechanism of retaining wall with backfill width (b=60) cm at soil friction angle Ø=300 and at angle of rock slope ß=700 for R.C wall

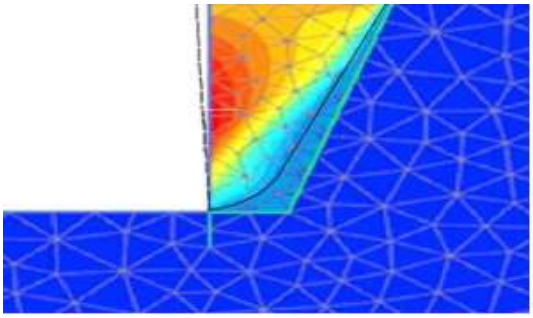

Fig. (45). Failure mechanism of retaining wall with backfill width (b=60) cm at soil friction angle Ø=300 and at angle of rock slope ß=80 for R.C wall

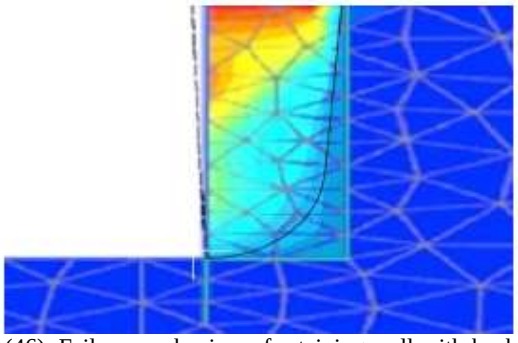

Fig. (46). Failure mechanism of retaining wall with backfill width (b=60) cm at soil friction angle Ø=300 and at angle of rock slope ß=900 for R.C wall

Based on the obtained results, the values of lateral earth pressure coefficient (K) are less than Rankine coefficient. In addition, Rankine theory was derived assuming the failure plane is linear with an inclination of [Ψ = 45 + (Ø/2)] with the horizontal as shown in Fig (42) [10]. Figs (43) to (50) show some examples of the shape and location of the failure mechanism obtained from finite element analysis.

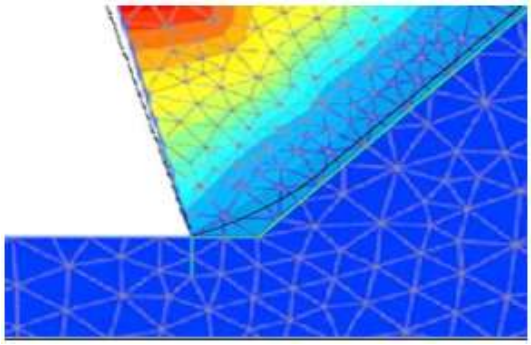

Fig. (47). Failure mechanism of retaining wall with backfill width (b=60) cm at soil friction angle Ø=300 and at angle of rock slope ß=60 for Masonry wall

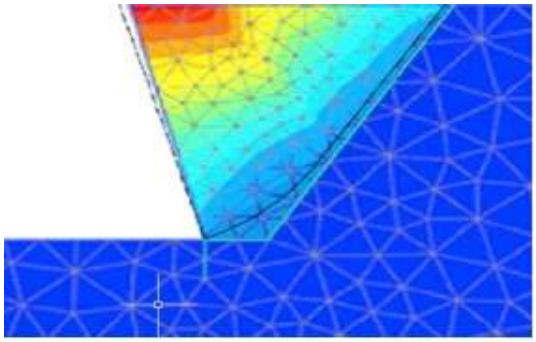

Fig. (48). Failure mechanism of retaining wall with backfill width (b=60) cm at soil friction angle Ø=300 and at angle of rock slope ß=700 for Masonry wall

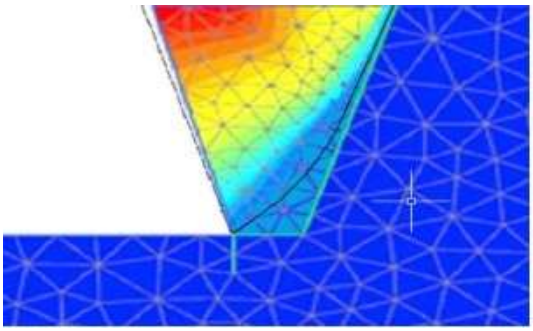

Fig. (49). Failure mechanism of retaining wall with backfill width (b=60) cm at soil friction angle Ø=300 and at angle of rock slope ß=800 for Masonry wall

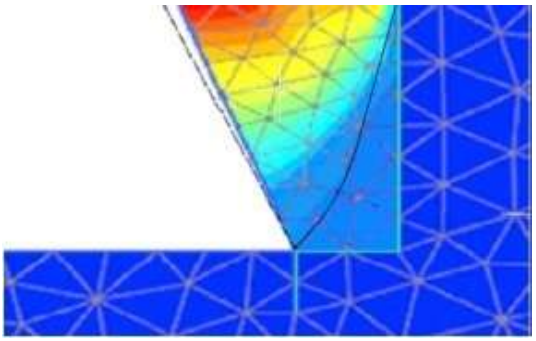

Fig. (50). Failure mechanism of retaining wall with backfill width (b=60) cm at soil friction angle Ø=300 and at angle of rock slope ß=900 for Masonry wall

Table (4) Values of tangent angels of the log a spiral portion originates from wall base for RC Wall.

No	angle of rock slope (β)	Angle of Internal Friction (Ø)	Obtained values of failure plane angle (α) by Finite Element			
			(b) = 40 cm	(b) = 50 cm	(b) = 60 cm	(b) = 70 cm
1	60^0	30^0	38.35	37.38	36.44	35.51
2		32^0	36.43	35.51	34.61	33.73
3		34^0	34.61	33.74	32.88	32.04
4		36^0	32.88	32.05	31.24	30.44
5		38^0	31.24	30.45	29.68	28.92
6	70^0	30^0	36.05	35.14	34.25	33.38
7		32^0	34.25	33.38	32.54	31.71
8		34^0	32.53	31.71	30.91	30.12
9		36^0	30.91	30.13	29.36	28.62
10		38^0	29.36	28.62	27.90	27.19
11	80^0	30^0	33.74	32.89	32.06	31.24
12		32^0	32.05	31.25	30.45	29.68
13		34^0	30.45	29.68	28.93	28.19
14		36^0	28.93	28.20	27.49	26.78
15		38^0	27.48	26.79	26.11	25.45
16	90^0	30^0	31.55	30.75	29.97	29.21
17		32^0	29.97	29.22	28.47	27.75
18		34^0	28.47	27.75	27.05	26.36
19		36^0	27.05	26.37	25.70	25.04
20		38^0	25.70	25.05	24.41	23.79

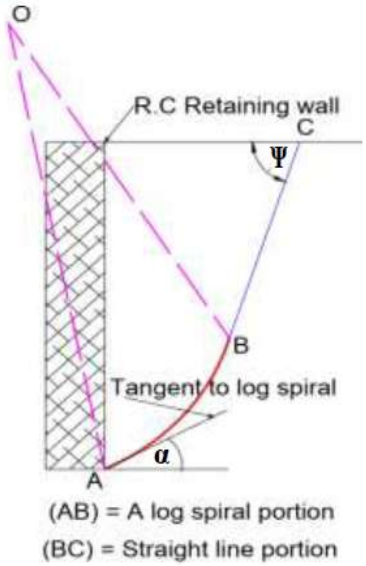

From the above results, it has clearly shown that the failure surface consists of a log spiral portion with a pole above the wall top and its tangent that inclined with different angles to the horizontal surface. However, the log spiral portion originates from the wall base with different tangent angles depending on the soil friction angle (Ø) and angle of rock slope (β). Tables (4) and (5) show the obtained values of failure plane angles.

In addition, it is clearly shown that the failure surface consists of a log spiral (AB) portion with a pole (O) above the wall top and its tangent that inclined with different angles with the horizontal surface (BC). However, the log spiral portion originates from the wall base (A) with different tangent angles. However, it is clearly shown that the tangent of the log spiral portion (BC) inclined with different angels to the horizontal surface depending on the soil friction angle (Ø) and angle of rock slope (β) as shown in Tables (6) and (7).

5.2) Effect of Backfill Dimensions and Friction Angles on Actual Plan of Failure Mechanism

Figs (51) to (58) show the failure surface for constrained (narrow) cohesionless backfill behind RC and Masonry walls compared with the inclination of the failure plane of Rankine theory.

Table (5) Values of tangent angels of the log a spiral portion originates from wall base for Masonry Wall.

No	angle of rock slope (β)	Angle of Internal Friction (Ø)	Obtained values of failure plane angle (α) by Finite Element			
			(b) = 40 cm	(b) = 50 cm	(b) = 60 cm	(b) = 70 cm
1	60^0	30^0	39.69	38.69	37.71	36.75
2		32^0	37.71	36.76	35.83	34.91
3		34^0	35.82	34.92	34.03	33.17
4		36^0	34.03	33.17	32.33	31.51
5		38^0	32.33	31.51	30.72	29.93
6	70^0	30^0	37.71	36.76	35.83	34.91
7		32^0	35.82	34.92	34.03	33.17
8		34^0	34.03	33.17	32.33	31.51
9		36^0	32.33	31.51	30.72	29.93
10		38^0	30.71	29.94	29.18	28.44
11	80^0	30^0	36.20	35.29	34.39	33.52
12		32^0	34.39	33.52	32.67	31.84
13		34^0	32.67	31.85	31.04	30.25
14		36^0	31.04	30.25	29.49	28.74
15		38^0	29.48	28.74	28.01	27.30
16	90^0	30^0	34.39	33.52	32.67	31.84
17		32^0	32.67	31.85	31.04	30.25
18		34^0	31.04	30.25	29.49	28.74
19		36^0	29.48	28.74	28.01	27.30
20		38^0	28.01	27.30	26.61	25.93

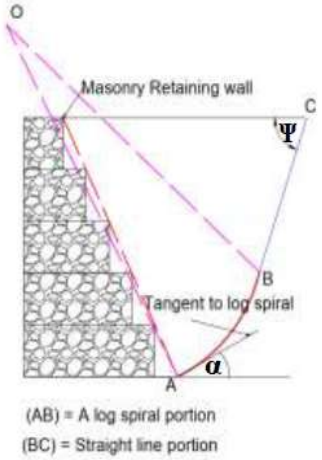

Table (6) Values of tangent angels of the log a spiral portion (straight-line portion "BC") that is inclined with the horizontal surface from wall base for RC Wall.

No	angle of rock slope (β)	Angle of Internal Friction (Ø)	Obtained values of failure plane angle (Ψ) by Finite Element			
			(b) = 40 cm	(b) = 50 cm	(b) = 60 cm	(b) = 70 cm
1	60^0	30^0	57.43	58.35	59.24	60.14
2		32^0	58.60	59.54	60.45	61.37
3		34^0	59.79	60.76	61.68	62.62
4		36^0	61.01	62.00	62.94	63.90
5		38^0	62.26	63.26	64.23	65.21
6	70^0	30^0	63.53	64.56	65.54	66.54
7		32^0	64.69	65.74	66.74	67.76
8		34^0	65.88	66.94	67.96	69.00
9		36^0	67.09	68.17	69.21	70.26
10		38^0	68.32	69.42	70.48	71.55
11	80^0	30^0	69.57	70.69	71.77	72.86
12		32^0	71.48	72.36	72.46	74.58
13		34^0	73.96	74.06	73.19	76.33
14		36^0	75.47	75.80	76.96	78.13
15		38^0	77.01	77.59	78.77	79.97
16	90^0	30^0	78.81	79.42	80.62	81.85
17		32^0	80.81	81.04	82.27	83.52
18		34^0	81.81	82.69	83.95	85.23
19		36^0	83.81	84.38	85.66	86.97
20		38^0	85.81	86.10	87.41	88.74

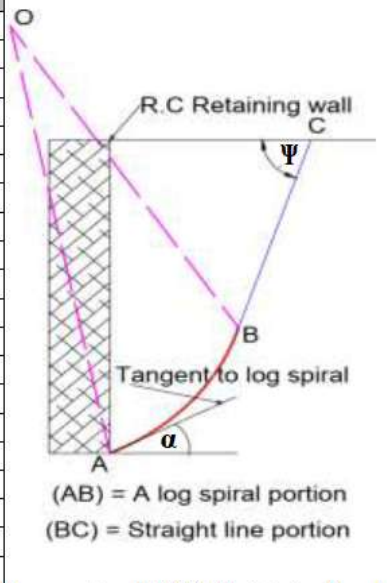

Table (7) Values of tangent angels of the log a spiral portion (straight-line portion "BC") that is inclined with the horizontal surface from wall base for Masonry Wall.

No	angle of rock slope (β)	Angle of Internal Friction (Ø)	Obtained values of failure plane angle (Ψ) by Finite Element			
			(b) = 40 cm	(b) = 50 cm	(b) = 60 cm	(b) = 70 cm
1	60^0	30^0	59.38	59.17	60.07	60.99
2		32°	60.59	60.38	61.30	62.23
3		34°	61.82	61.61	62.55	63.50
4		36°	63.08	62.87	63.83	64.80
5		38°	64.37	64.15	65.13	66.12
6	70^0	30^0	65.69	65.46	66.46	67.47
7		32°	66.89	66.66	67.68	68.71
8		34°	68.12	67.89	68.92	69.97
9		36°	69.36	69.13	70.18	71.25
10		38°	70.64	70.40	71.47	72.56
11	80^0	30^0	71.93	71.69	72.78	73.89
12		32°	73.40	73.37	74.49	75.63
13		34°	74.90	75.10	76.25	77.41
14		36°	76.43	76.87	78.04	79.23
15		38°	77.99	78.68	79.88	81.09
16	90^0	30^0	79.81	80.53	81.76	83.00
17		32°	81.81	82.18	83.43	84.70
18		34°	82.81	83.85	85.13	86.43
19		36°	84.81	85.56	86.87	88.19
20		38°	86.81	87.31	88.64	89.99

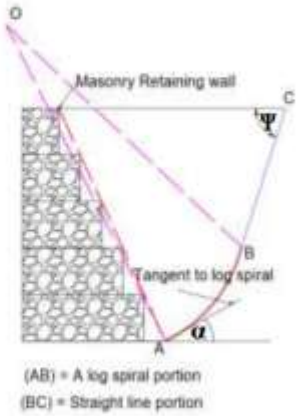

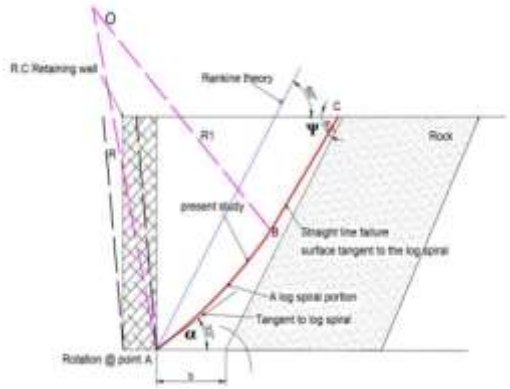

Fig (51). Actual failure plan for active condition for R.C wall at soil friction angle (Ø)= 34^0 at angle of rock slope (β) =60^0 and backfill width (b=60 cm).

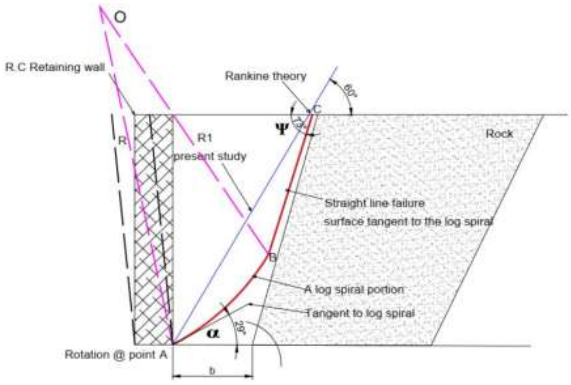

Fig (53). Actual failure plan for active condition for R.C wall at soil friction angle (Ø)= 34^0 at angle of rock slope (β) =80^0 and backfill width (b=60 cm).

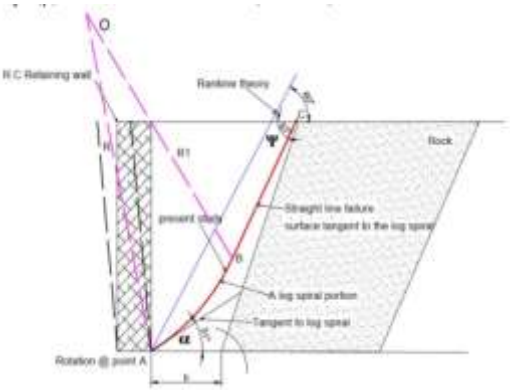

Fig (52). Actual failure plan for active condition for R.C wall at soil friction angle (Ø)= 34^0 at angle of rock slope (β) =70^0 and backfill width (b=60 cm).

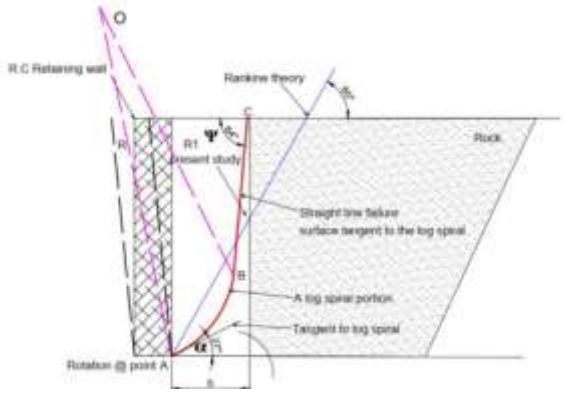

Fig (54). Actual failure plan for active condition for R.C wall at soil friction angle (Ø)= 34^0 at angle of rock slope (β) =90^0 and backfill width (b=60 cm).

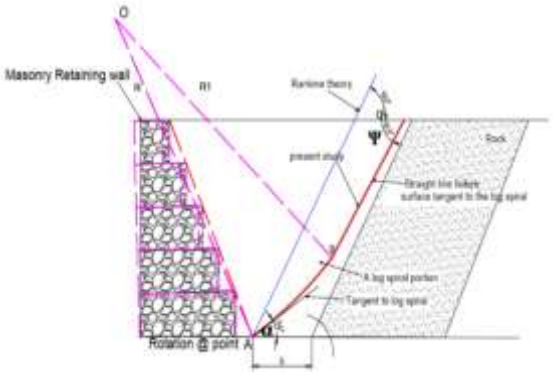

Fig (55). Actual failure plan for active condition for Masonry wall at soil friction angle (Ø)= 34^0 at angle of rock slope (β) =60^0 and backfill width (b=60 cm).

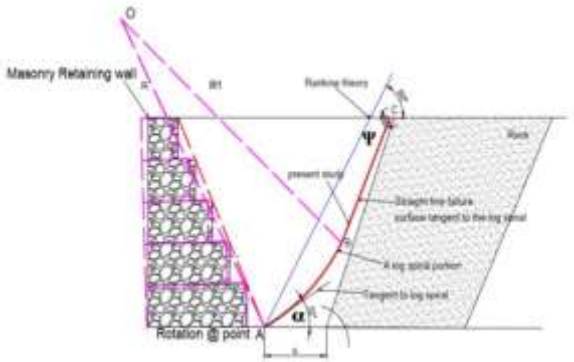

Fig (56). Actual failure plan for active condition for Masonry wall at soil friction angle (Ø)= 34^0 at angle of rock slope (β) =70^0 and backfill width (b=60 cm).

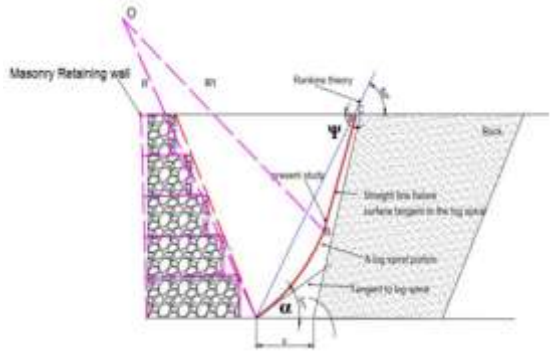

Fig (57). Actual failure plan for active condition for Masonry wall at soil friction angle (Ø)= 34^0 at angle of rock slope (β) =80^0 and backfill width (b=60 cm).

From the present study, the actual failure plane for constrained (narrow) cohesionless backfill is neither a straight line as Rankine theory nor inclined [Ψ = 45 + (Ø/2)] with the horizontal. The failure plane consists of a log spiral portion with a pole above the wall top and its tangent (BC) inclined with different angles to the horizontal surface. However, the log spiral portion originates from the wall base with different tangent angles depending on the soil friction angle (Ø) and angle of rock slope (β). In addition, the tangent of the log spiral portion (BC) inclined with different angels to the horizontal surface depending on soil friction angle (Ø) and angle of rock slope (β). However, the obtained results show fair agreement with the available solutions.

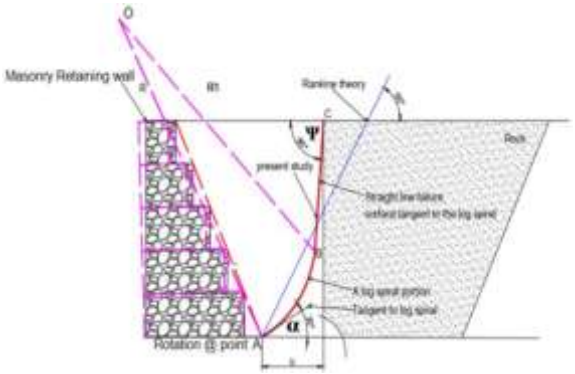

Fig (58). Actual failure plan for active condition for Masonry wall at soil friction angle (Ø)= 34^0 at angle of rock slope (β) =90^0 and backfill width (b=60 cm).

Conclusions

From the present study, the following conclusions are obtained:

i. The lateral earth pressure increases with increasing the constrained (narrow) backfill width and decreases with increasing the angle of rock slope.

ii. The coefficient of lateral earth pressure increases with increasing the constrained (narrow) backfill width and increasing with increasing width to height ratio of the wall.

iii. The lateral earth pressure coefficient (K) increases with decreasing soil friction angle (Ø) and decreases with increasing angle of rock slope (β).

iv. The lateral earth pressure coefficient (K) for masonry wall is higher than for RC wall.

v. The value of the coefficient of active earth pressures (K) is found to be 0.65 to 0.85 of Rankine coefficients (Kr).

vi. The failure plane consists of a log spiral portion with a pole above the wall top and its tangent inclined with different angles to the horizontal surface. However, the log spiral portion originates from the wall base with different tangent angles. In addition, the tangent of the log spiral portion inclined with different angels to the horizontal surface depending on the soil friction angle (Ø) and angle of rock slope (β).

vii. The obtained results show fair agreement with the available solutions.

References

1. M. Aubertin., L. Li, S. Arnoldi., T. Belem, B. Bussière, M. Benzaazoua, and R. Simon. (2003) "Interaction between backfill and rock mass in narrow stopes" Submitted to the Soil Rock2003: 12th Panamerican Conference on Soil Mechanics and Geotechnical Engineering and 39th U.S. Rock Mechanics Symposium. pp.1-8.
2. Leshchinsky, D., Hu, Y., & Han, J. (2003). "Design implications of limited reinforced zone space in SRW's". The 17th GRI Conference on Hot Topics in Geosynthetics IV. Las Vegas: Nevada.
3. Lawson, C., & Yee, T. (2005). "Reinforced soil retaining walls with constrained reinforced fill zones". *Geo-Frontiers.* ASCE Geo-Institute Conference.
4. Matthias Sperl "Experiments on corn pressure in silo cells – translation and comment of Janssen's paper from 1895," Granular Matter, Vol. 8, pp.59-65, December 2006.
5. Kniss, K.T, Yang, K.-H., Wright, S.G., and Zornberg, J.G. (2007). "Earth Pressures and Design Consideration of Narrow MSE Walls", Proceedings of the Conference of Texas Section-ASCE Meeting, Taylor, Texas, April, pp. 1-22 (CD-ROM). ASCE TEXAS Section, Spring Term, April, 2007.
6. Kuo-Hsin Yang and Chia-Nan Liu (2007) "Finite Element Analysis Of Earth Pressures For Narrow Retaining Walls" Journal of GeoEngineering, Vol. 2, No.2, pp. 43-52, Aug. 2007. Corresponding author), Department of Civil. Engineering, National Chi Nan University, Taiwan, 545, R.O.C. (e-mail: cnliu@ncnu.edu.tw).
7. Kame, G. S., Dewaiker, D. M., & Choudhury, D. (2010). Active Thrust on a Vertical Retaining Wall with Cohesionless Backfill. EJGE, 15, 1848-1862.
8. Eltayeb Hassan Onsa. (2015). "Lateral Earth Pressure between two Parallel Rigid Retaining Walls" International Journal of Scientific & Engineering Research, ISSN 2229-5518. Vol. 6, Issue 8, August-2015 pp.73-78. IJSER © 2015. http://www.ijser.org.
9. Gihan Abdelrahman., Youssef Gomaa. and Mohamed Kamel, (2017). "Behavior of Narrow Mechanically Stabilized Earth Walls" Proceedings of the 19th International Conference on Soil Mechanics and Geotechnical Engineering, Seoul 2017 pp. 1943-1964.
10. Das, B. (2011) Principles of Foundation Engineering. Pennsylvania: Christopher M. Shortt.

12/15/2018